Heliyon 10 (2024) e34715

Contents lists available at ScienceDirect

Heliyon

journal homepage: www.cell.com/heliyon

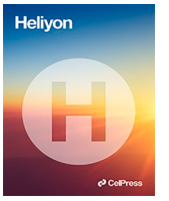

Research article

Zhiqiao Gancao decoction regulated JAK2/STAT3/ macrophage M1 polarization to ameliorate intervertebral disc degeneration

Zeling Huang [a,1], Xiaofeng Shen [a,b,1], Hua Chen [a,1], Zaishi Zhu [a], Binjie Lu [a], Long Zhang [a], Yujiang Liu [a], Yuwei Li [a,b,*], Bo Xu [a,**]

[a] Suzhou TCM Hospital Affiliated to Nanjing University of Chinese Medicine, Suzhou, Jiangsu, 215009, China
[b] Orthopaedic Traumatology Institute, Suzhou Academy of Wumen Chinese Medicine, Suzhou, Jiangsu, 215009, China

ARTICLE INFO

Keywords:
Intervertebral disc degeneration
Zhiqiao gancao decoction
Macrophage
Hyperalgesia
Polarization

ABSTRACT

Background: Zhiqiao Gancao decoction (ZQGCD) was created by Professor Gong Zhengfeng, a renowned Chinese medicine expert. Clinical studies have shown its efficacy in alleviating pain and enhancing lumbar function in intervertebral disc degeneration (IDD) patients. However, the precise mechanism of ZQGCD in treating IDD remains unclear.

Methods: The active components of ZQGCD were identified using Liquid chromatography-tandem mass spectrometry (LC-MS/MS). A rat model of intervertebral disc degeneration was established, and rats in each group received ZQGCD for three weeks. Assessment parameters included hyperalgesia status, observation of intervertebral disc tissue degeneration and macrophage infiltration, and analysis of JAK2/STAT3 pathway protein expression in the intervertebral disc. Primary macrophage M1 polarization was induced using LPS, with cells treated using the JAK2 inhibitor (AZD1480) and ZQGCD to evaluate macrophage polarization, cellular supernatant inflammatory factors, and JAK2/STAT3 pathway expression. Macrophage supernatant served as a conditioned medium to observe its effects on the proliferation of nucleus pulposus cells (NPCs) and the expression of collagen II and MMP3 proteins.

Results: A total of 81 active components were identified in ZQGCD. Following ZQGCD treatment, infiltrating macrophages in intervertebral disc tissues of model rats decreased, the content of M1 macrophages decreased, while the content of M2 macrophages increased, the expression of proinflammatory factors and pain-inducing factors in serum decreased, and the expression of substance P in intervertebral disc tissue decreased. Consequently, the intervertebral disc degeneration and hyperalgesia of rats were improved. In vitro studies revealed that LPS induced M1 macrophage polarization. By inhibiting the JAK2/STAT3 pathway, both JAK2 inhibitors and ZQGCD effectively suppressed M1 polarization, resulting in decreased levels of IL-1β, IL-6, TNF-α, and various other inflammatory factors. Consequently, this inhibition led to a delay in the degeneration of NPCs.

Conclusion: There is macrophage infiltration in the intervertebral disc tissue of IDD rats, and JAK2/STAT3 pathway is activated, macrophages are polarized to M1 type, resulting in

* Corresponding author. Suzhou Hospital of Traditional Chinese Medicine, 18 Yangsu Road, Canglang New City, Suzhou City, Jiangsu Province, China.
** Corresponding author. Suzhou Hospital of Traditional Chinese Medicine, 18 Yangsu Road, Canglang New City, Suzhou City, Jiangsu Province, China.
E-mail addresses: lyw97538@126.com (Y. Li), xubo12080@163.com (B. Xu).
[1] These authors have contributed equally to this work and share first authorship.

https://doi.org/10.1016/j.heliyon.2024.e34715
Received 26 February 2024; Received in revised form 13 July 2024; Accepted 15 July 2024
Available online 24 July 2024

inflammatory microenvironment, leading to intervertebral disc degeneration and hyperalgesia. ZQGCD exhibited a delaying effect on IDD and improved hyperalgesia by inhibiting the JAK2/STAT3/macrophage M1 polarization pathway.

1. Background

Low back pain (LBP) is a common condition affecting an estimated 637 million people globally [1]. Intervertebral disc degeneration (IDD) is identified as the primary cause of LBP, with up to 42 % of LBP cases attributed to disc disease [2]. In addition to the primary cause of partial or complete rupture of the intervertebral disc annulus due to mechanical injury, IDD is also linked to pathological changes in internal structures, such as inflammation [3]. The intervertebral disc comprises a central nucleus pulposus (NP), a peripheral annulus fibrosus (AF), and two adjacent cartilage endplates. From its formation, the nucleus pulposus has been enclosed within the AF and cartilage endplate to shield it from the body's immune system [4,5]. During the process of intervertebral disc degeneration, nerves, and blood vessels extend into the endplate and inner annulus along the fissure from the outer AF, creating migration channels for immune cells [6]. Macrophages are important cells activated by the human immune system, primarily playing roles in immune defense, immune homeostasis, and immune surveillance [7]. Research indicates that macrophages are the predominant cell type infiltrating degenerative intervertebral discs, exhibiting a positive correlation with the degree of disc degeneration [8,9], indicating that macrophages play a key role in disc degeneration.

Macrophages in tissues can perceive changes in their surrounding environment and adopt two phenotypes: M1 and M2. The M1 phenotype is pro-inflammatory, releasing tumor necrosis factor-α (TNF-α), interleukin (IL)-1β, and other pro-inflammatory factors, initiating an inflammatory response in downstream immune cells, creating an inflammatory microenvironment, and hastening the disease progression. Conversely, M2 is an anti-inflammatory phenotype that secretes anti-inflammatory factors, promoting tissue repair [10]. Increasing evidence suggests that macrophages, as inflammatory cells, may directly play a phagocytic role or regulate intervertebral disc metabolism through a synergistic neuro-immune mechanism. Dysfunction of macrophages may disrupt microenvironment homeostasis in the intervertebral disc, leading to the aggregation, chemotaxis, and diffusion of inflammatory factors, ultimately resulting in intervertebral disc degeneration [11–13]. Inflammatory factors, such as TNF-α, not only promote the release of inflammatory neuropeptides like substance P and Calcitonin Gene-Related Peptide (CGRP) at the peripheral nerve endings of the intervertebral disc but also enhance neuronal excitability, amplifying the perception of nociceptive stimuli and causing hyperalgesia in the body [14].

Zhiqiao Gancao decoction (ZQGCD) a decoction developed by Professor Gong Zhengfeng, a well-known Chinese medicine specialist, is widely recognized for its ability to eliminate blood stasis, clear blockages in the body's channels, and alleviate discomfort. Clinical studies demonstrate that ZQGCD, alone or combined with foraminoscopy and other therapies, effectively alleviates pain and improves lumbar function in patients with lumbar disc herniation and lumbar degeneration [15–19], with significant therapeutic efficacy. Basic studies further reveal that ZQGCD significantly reduces the levels of inflammatory factors such as IL-1β, IL-6, and TNF-α and chemokines such as C–C motif chemokine 2 (CCL2) in model rats, delay intervertebral disc degeneration, and alleviates hyperalgesia in model rats [20–22]. Building on this foundation, this study further explored the effect mechanism of ZQGCD in the treatment of IDD in rats. The results show M1 polarization of macrophages in the degenerative disc in rats, and ZQGCD can inhibit M1 polarization of macrophages by regulating the JAK2/STAT3 pathway, alleviating the inflammatory microenvironment of the disc, delaying IDD, and alleviating hyperalgesia.

Table 1
Components of ZQGCD.

Chinese Name	Providers	English name	Source	Proportion (g)
Zhiqiao	230307010 Tianling Herbal Decoction Piece Co., LTD, Suzhou, China	Aurantii fructus	Citrus aurantium L.	10
Danggui	230411 Chunhui Tang Co., LTD, Suzhou, China	Angelicae sinensis radix	Angelica sinensis (Oliv.) Diels	10
Dansen	20230203-C5 Tongde Pharmaceutical Co., LTD, Guizhou, China	Radix salviae miltiorrhizae	Salvia miltiorrhiza Bge.	10
Sanleng	221021 Chunhui Tang Co., LTD, Suzhou, China	Sparganii rhizoma	Sparganium stoloniferum Buch.-Ham.	10
Ezhu	221025 Chunhui Tang Co., LTD, Suzhou, China	Curcumae rhizome	Curcuma phaeocaulis Val. , Curcuma kwangsiensis S. G. Lee et C. F.Liang, or Curcuma wenyujin Y. H. Chen et C.Ling	10
Heichou	220906006 Tianling Herbal Decoction Piece Co., LTD, Suzhou, China	Pharbitidis	Pharbitis nil (L.) Choisy or Pharbitis purpurea (L.) Voigt	6
Baichou	211227006 Tianling Herbal Decoction Piece Co., LTD, Suzhou, China	Pharbitis purpurea	Pharbitis nil (L.) Choisy or Pharbitis purpurea (L.) Voigt	6
Gancao	230207 Chunhui Tang Co., LTD, Suzhou, China	Glycyrrhizae radix et rhizoma	Glycyrrhiza uralensis Fisch., Glycyrrhiza inflata Bat., or Glycyrrhiza glabra L.	6

AZD1480 (S2162-07, Selleck) is a novel, ATP-competitive JAK2 inhibitor dissolved in 40 % dimethyl sulfoxide.

2. Material and methods

2.1. Materials

2.1.1 Animals Sprague-Dawley (SD) rats weighing 160–180 g or 220–250 g were obtained from Shanghai SLAC Laboratory Animal Co., Ltd. Food and water were freely available to the rats under controlled conditions (25 °C, 50 % relative humidity).

2.1.2 Experimental drugs Suzhou TCM Hospital granted approval to ZQGCD. The drug composition is shown in Table 1. Combine all the medications with 500 mL of chilled water, let them soak for 1 h, then boil for 30 min before straining the mixture. Pour 300 mL of chilled water into the sediment, simmer for 30 min, and strain the resulting medicinal broth. Two batches of filtrates were mixed, and concentrate into 1 g/mL crude drug.

2.1.3 Experimental reagents Methanol (67-56-1, LC-MS category, CNW Technologies), Acetonitrile (75-05-8, LC-MS category, CNW Technologies), Formic acid (64-18-6), LC-MS quality, SIGMA), L-2-chloro-lphenylalanine (103616-89-3, ≥98 %, Shanghai Hengbo Biotechnology Co., LTD.), Enzyme-linked immunosorbent assay (ELISA) kits for IL-1β, IL-4, IL-6, IL-10, PGE2, and TNF-α (LA167616H, LA166619H, LA160102H, LA166608H, LA182217H, LA166601H) were obtained from Nanjing Lapda Biotechnology Co., LTD. HRP-labeled Affinipure Goat Anti-Rabbit IgG (H + L), β-Actin Antibody, MMP3 Antibody, collagen II Antibody (SA00001-2, SA00001-1, 20536-1-AP, 17873-1-AP, 2845-1AP, Proteintech) Substance P Antibody, iNOS Antibody, JAK2 Antibody, STAT3 Antibody, Phospho-STAT3 Antibody (DF7522, AF0199, AF6022, AF6294, AF3293, affbiotech); Phospho-JAK2-Y1007/1008 Antibody (AP0531, abclonal),and other similar products.

2.1.4 Experimental instruments The instruments used include a CO_2 constant temperature incubator (3111, Thermo Fisher Scientific, MA, USA), biosafety cabinet (BHC–1300IIB2, Suzhou Jinjing Purifying Equipment Co., LTD, Suzhou, Chian), flow cytometer (Accuri C6, BD, CA, USA), fluorescence microscope (DM6000B, Leica, Wetzlar, Germany), and mechanical pain sensitivity Measuring Instrument (BME-404, Chinese Academy of Medical Sciences, Beijing, China). Thermal pain sensing instrument (35150-001, Ugo Basil SLR, Italy), electric heating oven (101AS-3, Shanghai Shengxin Scientific Instrument Co., LTD. Shanghai, China), digital Pathology biopsy Scanner (VS200 Olympus, Tokyo, Japan); Tianping (E200 Sartorius Gottingen Germany); Table thermostatic oscillator (THZ-312 Shanghai Jinghong Experimental Equipment Co., LTD., Shanghai, China); ELx 800 light absorption enzyme label instrument, ELx 50 microporous plate automatic washing machine (BIOTEK VT USA), frozen Centrifuge (5424R Eppendorf Hamburg, Germany), thermostatic incubator (GHP-9050 N Shanghai Yiheng Scientific Instrument Co., LTD., Shanghai, China), light cycle 96, enzyme label instrument, Mini-PROTEAN Tetra, PowerPac Power supply (biorad, CA, USA), and chemiluminescence imaging system (Tanon 5200, Shanghai Tieneng Technology Co., LTD., Shanghai, China) were also used in this experiment.

2.2. Liquid chromatography-tandem–mass spectrometer (LC-MS/MS)

The 100 μL of ZQGCD was accurately pipetted into a 1.5 mL centrifuge tube.Subsequently, 300 μL of the extraction solution was added. Following 30 s of vortex mixing, ultrasonic extraction was carried out at a low temperature for a duration of 30 min (5 °C, 40 kHz). Afterwards, the specimen was kept in a freezer at a temperature of −20 °C for a duration of 30 min. Afterwards, the supernatant was eliminated by centrifuging for 15 min at a temperature of 4 °C and a speed of 13000 g, and subsequently dried using nitrogen. To dissolve again, 100 μL of a mixture was added, and the solution was mixed vigorously for 30 s. After extracting with low-temperature ultrasound for 5 min (at 5 °C and 40 KHz), the mixture was centrifuged for 10 min (at 13000 g and 4 °C) to eliminate the liquid above the sediment. The resulting liquid was then transferred to the injection vial using an internal tube for machine analysis. Furthermore, 20 μL of supernatant was added to each sample as a quality control sample. The Thermo Field's Vanquish UHPLC-Q Exactive HF-X system from Thermo Fisher Scientific was used as the instrument platform for conducting the LC-MS analysis, which involved ultra-high performance liquid chromatography-tandem Fourier Transform mass spectrometry. The volume of the sample was 3 μL, and the temperature of the column was kept at 40 °C. The mass spectrum was obtained using electrospray ionization, with signals collected in both positive and negative ion scanning modes. The unprocessed data were imported into ProgenesisQI, a metabolomics processing software developed by WatersCorporation in Milford, USA. The software was used for tasks such as baseline filtering, peak identification, integration, retention time correction, and peak alignment. In the end, a data matrix was acquired which included retention time, mass-charge ratio, peak intensity, and additional details. Afterwards, the software was utilized to detect the distinctive peak database, in which the MS and MS/MS mass spectrum data was compared with the metabolic database. Metabolites were identified by matching the secondary mass spectrum score, with the MS mass error being limited to below 10 ppm.

2.3. Animals and experiment

Fifty SD rats were randomly assigned to the IDD group (40 rats) and the sham operation group (10 rats). Rats were anesthetized with a 1 ml/kg intraperitoneal injection of 3 % pentobarbital. They were fixed in the supine position, and the skin was prepared and disinfected with the midline of the abdomen as the center. The location of the L4-5 intervertebral disc was determined via an anterior approach through a midline abdominal incision. A 21G puncture needle was selected, inserted into the anterolateral parallel cartilaginous endplate at a 45° angle for approximately 3 mm, and then withdrawn after remaining in place for 10 s [23]. The rat's abdominal cavity was sutured layer by layer. In the sham operation group, only the abdominal cavity was exposed, and no puncture of the intervertebral disc occurred. After 5 days of modeling, drug intervention commenced as follows: the Sham group and Model group, received no drug intervention; ZQGCD low dose, ZQGCD medium dose, and ZQGCD high dose groups (ZQGCD-L, ZQGCD-M, and ZQGCD-H) were orally administered ZQGCD at doses of 3.06 g/kg, 6.12 g/kg, and 12.24 g/kg, respectively, starting on the 5th day

after modeling for 3 weeks. The paw withdrawal threshold (PWT) and paw retraction latency (PWL) were assessed before and on the 7th, 14th, 20th, and 25th days after modeling. After the experiment, 3 % pentobarbital sodium anesthesia was administered, blood was collected from the abdominal aorta, and L4-5 intervertebral disc tissue was rapidly separated. A portion was fixed in 4 % paraformaldehyde, and another part was stored in a cryogenic refrigerator at −80 °C for later use.

2.4. Preparation of ZQGCD-containing serum

For seven consecutive days, rats in the group that received serum containing ZQGCD were administered ZQGCD (12.24 mL/kg/d) orally. Blood was drawn from the abdominal aorta. The blood samples underwent centrifugation at 3000 r/min for 15 min. The supernatant was obtained and the mixture was filtered and stored at −80 °C after water bathing at 56 °C.

2.5. Extraction, culture, and treatment of macrophages

The SD rats were euthanized, and the necks were disinfected with alcohol for 2min. 15 mL of PBS was injected into the abdominal cavity, and abdominal massage facilitated the extraction of peritoneal macrophages. After resting for 2–3 min, the peritoneal lavage solution was obtained through centrifugation, with the supernatant discarded. High-glucose DMEM medium containing 10 % FBS was suspended on a 6-well plate, and after 3 h, adherent purified macrophages were obtained, and the supernatant was aspirated. After washing with sterile PBS three times, the cells were added to the culture for further cultivation.

Initially, the effects of different concentrations of ZQGCD-containing serum (0 %, 5 %, 10 %, 15 %, and 20 %) on macrophage proliferation and migration were observed. Subsequently, macrophages were divided into the Control group, LPS group, AZD1480+LPS group, and drug-containing serum group with various concentrations. The intervention conditions were as follows. In the Control group, 10 % blank serum was cultured for 24 h. In the LPS group, macrophage M1 polarization was induced by culturing with 10 % biank serum for 24 h, supplemented with 1ug/mL Lipopolysaccharides (LPS). In the AZD1480+LPS group, 5uM AZD1480 was added to the LPS group. In the 5 % ZQGCD + LPS group, macrophage M1 polarization was induced by culturing with 5 % ZQGCD-containing serum for 24 h and 1ug/mL LPS added. Similarly, in the 10%ZQGCD + LPS group, macrophage M1 polarization was induced by culturing with 10 % ZQGCD-containing serum for 24 h and 1ug/mL LPS. In the 15 % ZQGCD + LPS group, macrophage M1 polarization was induced by culturing with 15 % ZQGCD-containing serum for 24 h and 1ug/mL LPS. The cell supernatant of each group was collected, mixed at a 1:1 ratio with DMEM/F12 medium, and supplemented with 10 % fetal bovine serum as conditioned medium (CM) for the culture of nucleus pulposus cells (NPCs).

2.6. Extraction, culture, and treatment of NPCs

The SD rats were euthanized, and their necks were disinfected with alcohol for 2min. The tail was severed, and the tail skin was peeled off and soaked in alcohol before transfer to a benchtop. The intervertebral disc tissue was incised, and the nucleus pulpoeus was carefully removed using curettles, and subsequently cut into approximately 1 mm^3 fragments. The remaining tissue residue was digested with 0.2 % type II collagenase at 37 °C for 2 h, followed by filtration through a sterile 200-mesh screen. After centrifugation, the cells were re-suspended in a DMEM/F12 cell medium containing 10 % FBS and 1 % double-antibody. Subsequently, they were cultured in a constant temperature incubator at 37 °C and 5 % CO2. The medium was changed every 3 days, and when cell confluence reached 80 %–90 %, trypsin (0.25 %) was employed for digestion and passaging.

The second generation NPCs were selected and categorized into the Control-CM group, LPS-CM group, (AZD1480+LPS)-CM group, (5%ZQGCD + LPS) group, (10%ZQGCD + LPS)-CM group, and (15%ZQGCD + LPS)-CM group. They were then added to the corresponding groups of macrophage conditional medium for culture. NPC activity was assessed at 12 h, 24 h, 36 h, and 48 h, while the expression of collagen II and Matrix metalloproteinase-3 (MMP3) in NPCs was evaluated 48 h later.

2.7. Behavioral Testing

Mechanical allodynia, defined as the 50 % paw withdrawal threshold (PWT), was assessed using the Von Frey hair (Touch Test Sensory Evaluators, North Coast Medical, Inc.). The Von Frey wire was used to daily test the foot withdrawal threshold. The minimum grams eliciting at least five positive reactions determined the foot withdrawal threshold. Stimulation commenced with the minimum amount and gradually increased in intensity.

The thermal sensitivity of the hind paw plantar surface was assessed by measuring the paw retraction latency (PWL). A cold and hot plate pain meter (XR1100, Shanghai Xinruan Information Technology Co., LTD) was used, with the temperature set at 55 °C. To avoid causing significant harm to the rats due to the thermal light source, the maximum time allowed for thermal stimulation was restricted to 20 s. Each rat underwent three times, and the results were presented as average values.

2.8. Hematoxylin-eosin (HE) staining

Following routine dewaxing, intervertebral disc sections were stained according to kit instructions. Histological examination was conducted on each section using a light microscope, and subsequent grading was carried out. The scoring included four items: AF structure, the boundary line between AF and NP, matrix in NP, and cells in NP. The scoring of each item ranged from 1 to 3, with a

maximum cumulative score of 12 [24].

2.9. Enzyme-linked immunosorbent assay (ELISA)

ELISA kits were used to evaluate the levels of IL-1β, IL-4, IL-6, IL-10, PGE2, and TNF-α in serum, along with IL-1β, IL-6, and TNF-α in macrophage supernatant. Initially, a standard curve was generated, incorporating blank wells, standard wells, and sample wells. Subsequently, samples were added sequentially, followed by an incubation at 37 °C for 90 min. The plates were then washed, and the working antibody solution was applied, incubated for 60 min, and followed by another wash. The solution containing the enzyme was applied, left for 30 min, and then the plates were rinsed once more. The solution for color development was introduced and left in darkness for a duration of 15 min. Subsequently, the optical density was determined utilizing an enzyme-labeled device (BIOTEK, VT, USA).

2.10. Cell counting Kit-8 (CCK-8) assay

The proliferative activity of macrophages and NPCs was evaluated using CCK8. To conduct group intervention, cells were placed in 96-well plates and 10 μl of CCK-8 solution was introduced into each well to evaluate cell viability. After incubating for 60 min, the absorbance of each well was measured at a wavelength of 450 nm.

2.11. Immunofluorescence

Multiplex immunofluorescence was used to detect macrophage infiltration in the intervertebral disc and macrophage polarization. Monochromatic immunofluorescence was used to determine the expression levels of collagen II and MMP3 in NPCs. Tissues or cells were routinely permeabilized and subsequently blocked. CD68 antibody (1:200), iNOS antibody (1:200), Arg-1 antibody (1:500), collagen II antibody (1:500), and MMP3 antibody (1:600) were added and incubated overnight at 4 °C. The following day, the secondary antibody was added and incubated at room temperature for 30 min. DAPI was used for counterstaining, and observations were performed under a fluorescence microscope (DM6000B, Leica, Wetzlar, Germany).

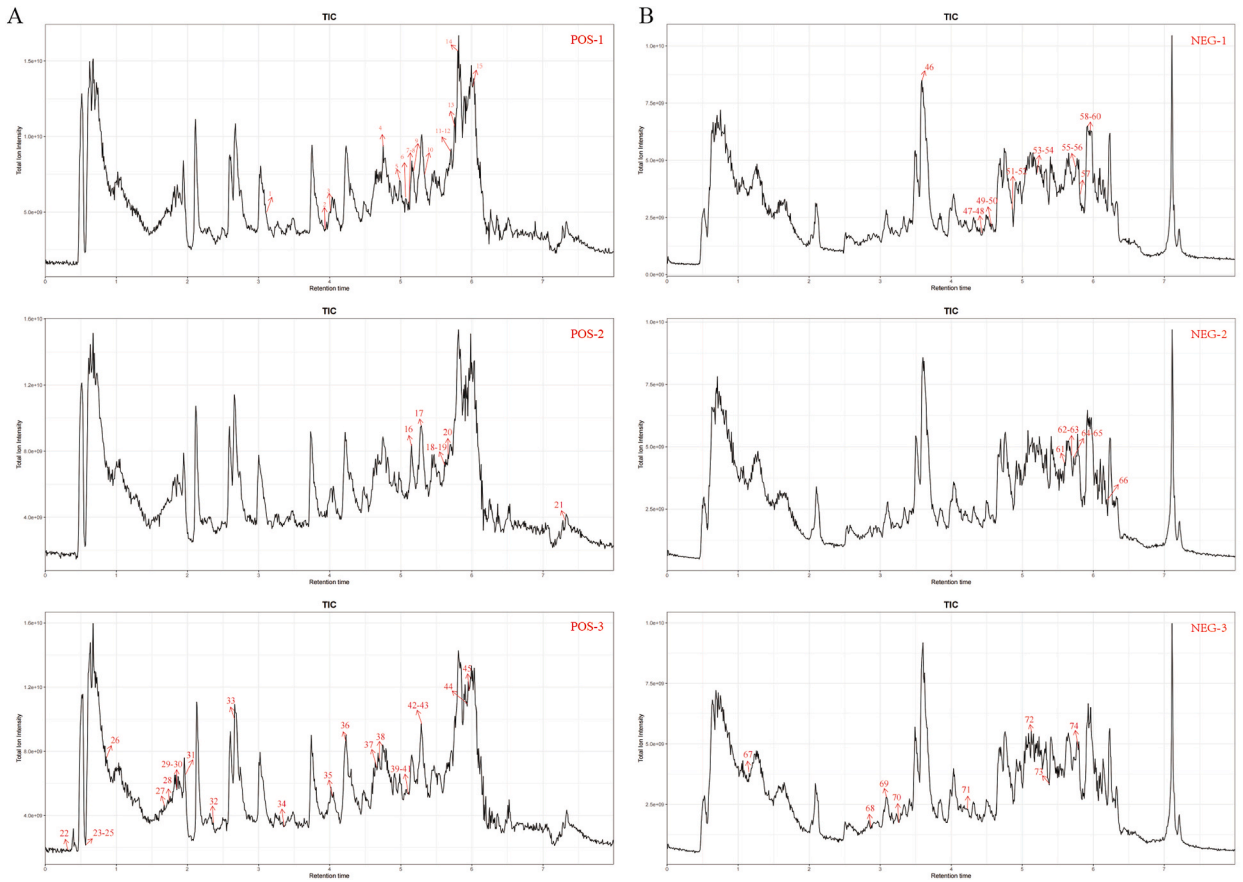

Fig. 1. Ion flow diagram for detecting the composition of ZQGCD. (A): Positive ion mode; (B): Negative ion mode.

Table 2
Characteristics of constituents of ZQGCD.

NO.	Identification	Molecular formula	Reserve time	Mode	classification	Affiliation
1	Pinocembrin	C15H12O4	3.082	pos	PPs	Glycyrrhizae
2	Isoorientin	C21H20O11	3.912	pos	PPs	Radix salviae miltiorrhizae
3	Calycosin	C16H12O5	4.028	pos	PPs	Glycyrrhizae, Angelicae sinensis radix
4	Hesperetin	C16H14O6	4.751	pos	PPs	Fructus aurantii
5	Baicalin	C21H18O11	5.000	pos	PPs	Radix salviae miltiorrhizae
6	Prunetin	C16H12O5	5.031	pos	PPs	Glycyrrhizae
7	Isoliquiritin apioside	C26H30O13	5.054	pos	PPs	Glycyrrhizae
8	Ononin	C22H22O9	5.124	pos	PPs	Glycyrrhizae
9	Isokaempferide	C16H12O6	5.272	pos	PPs	Glycyrrhizae
10	Isoliquiritin	C21H22O9	5.334	pos	PPs	Glycyrrhizae
11	Chrysoeriol	C16H12O6	5.732	pos	PPs	Radix salviae miltiorrhizae
12	Galangin	C15H10O5	5.747	pos	PPs	Glycyrrhizae
13	Sinensetin	C20H20O7	5.755	pos	PPs	Fructus aurantii
14	Psoralen	C11H6O3	5.810	pos	PPs	Angelicae sinensis radix
15	Kanzonol Z	C25H26O5	5.980	pos	PPs	Glycyrrhizae
16	Caffeate	C9H8O4	1.9575	pos	PPs	Pharbitidis, Pharbitis purpurea
17	Narirutin	C27H32O14	4.6419	pos	PPs	Fructus aurantii
18	Angelicin	C11H6O3	5.155	pos	Lipids and lipid-like molecules	Angelicae sinensis radix
19	Cuminaldehyde	C10H12O	5.287	pos	Lipids and lipid-like molecules	Angelicae sinensis radix
20	Gibberellin A8	C19H24O7	5.529	pos	Lipids and lipid-like molecules	Pharbitidis, Pharbitis purpurea
21	Eucarvone	C10H14O	5.568	pos	Lipids and lipid-like molecules	Angelicae sinensis radix
22	Furanodiene	C15H20O	5.630	pos	Lipids and lipid-like molecules	Curcumae rhizome
23	Tanshinone IIA	C19H18O3	6.1035	pos	Lipids and lipid-like molecules	Radix salviae miltiorrhizae
24	Germacrone	C15H22O	6.5377	pos	Lipids and lipid-like molecules	Curcumae rhizome
25	Oleamide	C18H35NO	7.318	pos	Lipids and lipid-like molecules	Angelicae sinensis radix
26	Butanal	C4H8O	0.373	pos	OOC	Angelicae sinensis radix
27	L-Alanine	C3H7NO2	0.613	pos	Organic acids and derivatives	Angelicae sinensis radix
28	Prunasin	C14H17NO6	0.658	pos	OOC	Fructus aurantii
29	L-Proline	C5H9NO2	0.673	pos	Organic acids and derivatives	Angelicae sinensis radix
30	Furfural	C5H4O2	0.873	pos	OOC	Pharbitidis, Pharbitis purpurea, Angelicae sinensis radix
31	4-Hydroxybenzaldehyde	C7H6O2	1.726	pos	OOC	Rhizoma sparganii
32	Phenol	C6H6O	1.819	pos	Benzenoids	Angelicae sinensis radix
33	Adenosine	C10H13N5O4	1.865	pos	Nucleosides, nucleotides, and analogues	Angelicae sinensis radix
34	Guanosine	C10H13N5O5	1.896	pos	Nucleosides, nucleotides, and analogues	Angelicae sinensis radix
35	Estragole	C10H12O	1.950	pos	Benzenoids	Fructus aurantii, Glycyrrhizae
36	Ephedrine	C10H15NO	2.433	pos	Benzenoids	Fructus aurantii
37	Indole	C8H7N	2.673	pos	Organoheterocyclic compounds	Angelicae sinensis radix
38	Phthalic Acid	C8H6O4	3.322	pos	Benzenoids	Angelicae sinensis radix
39	Tyramine	C8H11NO	4.052	pos	Benzenoids	Fructus aurantii
40	Cnidilide	C12H18O2	4.223	pos	Organoheterocyclic compounds	Angelicae sinensis radix
41	Gallic Acid	C7H6O5	4.658	pos	Benzenoids	Glycyrrhizae
42	Neohesperidin	C28H34O15	4.751	pos	PPs	Fructus aurantii
43	Licorice glycoside A	C36H38O16	5.124	pos	Organoheterocyclic compounds	Glycyrrhizae
44	Fustin	C15H12O6	5.132	pos	Benzenoids	Fructus aurantii
45	Dimethyl Phthalate	C10H10O4	5.171	pos	Benzenoids	Angelicae sinensis radix
46	Benzaldehyde	C7H6O	5.287	pos	Benzenoids	Pharbitidis, Pharbitis purpurea
47	Ligustilide	C12H14O2	5.287	pos	Organoheterocyclic compounds	Angelicae sinensis radix
48	Salicylic Acid	C7H6O3	5.934	pos	Benzenoids	Fructus aurantii
49	Embelin	C17H26O4	5.965	pos	OOC	Pharbitidis, Pharbitis purpurea

(*continued on next page*)

Table 2 (*continued*)

NO.	Identification	Molecular formula	Reserve time	Mode	classification	Affiliation
50	Umbelliferone	C9H6O3	3.602	neg	PPs	Fructus aurantii, Angelicae sinensis radix
51	Medicarpin	C16H14O4	4.479	neg	PPs	Glycyrrhizae
52	Neoeriocitrin	C27H32O15	4.495	neg	PPs	Fructus aurantii
53	Scopoletin	C10H8O4	4.551	neg	PPs	Angelicae sinensis radix
54	Esculetin	C9H6O4	4.551	neg	PPs	Fructus aurantii, Glycyrrhizae, Angelicae sinensis radix
55	Ferulic Acid	C10H10O4	4.814	neg	PPs	Fructus aurantii, Pharbitidis, Pharbitis purpurea, Angelicae sinensis radix, Radix salviae miltiorrhizae, Rhizoma sparganii
56	Kaempferide	C16H12O6	4.838	neg	PPs	Fructus aurantii
57	Diosmin	C28H32O15	5.252	neg	PPs	Fructus aurantii
58	Rosmarinic Acid	C18H16O8	5.323	neg	PPs	Radix salviae miltiorrhizae
59	Glycyrol	C21H18O6	5.713	neg	PPs	Glycyrrhizae
60	Phaseollidin	C20H20O4	5.793	neg	PPs	Pharbitidis, Pharbitis purpurea
61	Phaseollinisoflavan	C20H20O4	5.889	neg	PPs	Glycyrrhizae
62	Uralenol	C20H18O7	5.913	neg	PPs	Glycyrrhizae
63	3-Hydroxyglabrol	C25H28O5	5.945	neg	PPs	Glycyrrhizae
64	Morusin	C25H24O6	5.992	neg	PPs	Glycyrrhizae
65	Azelaic Acid	C9H16O4	5.610	neg	Lipids and lipid-like molecules	Angelicae sinensis radix
66	Licoricesaponin J2	C42H64O16	5.674	neg	Lipids and lipid-like molecules	Glycyrrhizae
67	Tiglic acid	C5H8O2	5.689	neg	Lipids and lipid-like molecules	Pharbitidis, Pharbitis purpurea
68	Limonin	C26H30O8	5.721	neg	Lipids and lipid-like molecules	Glycyrrhizae
69	Licoricesaponin G2	C42H62O17	5.793	neg	Lipids and lipid-like molecules	Glycyrrhizae
70	Falcarindiol	C17H24O2	6.104	neg	Lipids and lipid-like molecules	Glycyrrhizae
71	Citric Acid	C6H8O7	1.294	neg	Organic acids and derivatives	Fructus aurantii, Angelicae sinensis radix
72	Benzoic acid	C13H14O8	2.891	neg	OOC	Fructus aurantii
73	Chlorogenic Acid	C16H18O9	3.100	neg	OOC	Pharbitidis, Pharbitis purpurea, Angelicae sinensis radix, Radix salviae miltiorrhizae
74	P-Anisic Acid	C8H8O3	3.211	neg	Benzenoids	Angelicae sinensis radix
75	Kanokoside C	C27H42O17	3.7357	neg	OOC	Glycyrrhizae radix et rhizoma
76	Kanokoside A	C21H32O12	3.7516	neg	Organic acids and derivatives	Glycyrrhizae radix et rhizoma
77	Maltol	C6H6O3	4.183	neg	Organoheterocyclic compounds	Angelicae sinensis radix
78	Phthalide	C8H6O2	5.133	neg	Organoheterocyclic compounds	Angelicae sinensis radix
79	Hispidulin	C16H12O6	5.363	neg	PPs	Glycyrrhizae
80	Salvianolic Acid B	C36H30O16	5.4029	neg	PPs	Radix salviae miltiorrhizae
81	Diethyl Phthalate	C12H14O4	5.761	neg	Benzenoids	Fructus aurantii

Note: PPs: Phenylpropanoids and polyketides, OOC: organic oxygen compounds.

2.12. Western blot

The expression levels of JAK2, *p*-JAK2, STAT3, p-STAT3, substance p, and iNOS protein in rat intervertebral disc tissue were detected using Western blotting. Additionally, the expression levels of JAK2, *p*-JAK2, STAT3, and p-STAT3 proteins were examined in macrophages. At first, the samples were subjected to protein extraction, and the concentration of protein was assessed utilizing the BCA technique. The proteins were then denatured by heating in a constant-temperature metal bath. Afterwards, additional samples were included according to the protein concentration, subjected to electrophoresis, and then transferred onto a PVDF membrane. At room temperature, the membrane was sealed using 5 % skim milk powder. The following antibodies were added and incubated at 4 °C overnight: JAK2 antibody (1:1000), *p*-JAK2 antibody (1:1500), STAT3 antibody (1:1000), p-STAT3, substance P antibody (1:1000), iNOS antibody (1:1500), and β-actin antibody (1:5000). On the subsequent day, the second antibody was administered and left to incubate for a duration of 60 min. Finally, ECL chromogenic solution was used for exposure.

2.13. Statistical analysis of data

GraphPad Prism 9.0.0 was used for statistical analysis. One-way analysis of variance (ANOVA) was used to compare multiple groups, and pairwise comparisons were conducted using Tukey's test. $P < 0.05$ was considered statistically significant.

3. Results

3.1. ZQGCD composition analysis

A total of 1167 active ingredients were identified using LC-MS/MS (positive ion mode: 602; negative ion mode: 565), as illustrated in Fig. 1A and B. Upon comparison with TCMSP, TCMID, and other TCM databases, a total of 81 components specific to ZQGCD were identified (positive ion mode: 49; negative ion mode: 32), originating from Fructus aurantii (n = 20), Angelicae sinensis radix (n = 23), Radix salviae miltiorrhizae (n = 8), Rhizoma sparganii (n = 2), Curcumae rhizome (n = 2), Pharbitidis (n = 9), Pharbitis purpurea (n = 9), and Glycyrrhizae (n = 25). These 81 compounds encompassed Phenylpropanoids and polyketides (n = 35), Benzenoids (n = 12), Lipids and lipid-like molecules (n = 14), Nucleosides, nucleotides, and analogues (n = 2), Organic acids and derivatives (n = 4), Organic oxygen compounds (n = 8), and Organoheterocyclic compounds (n = 6), as detailed in Table 2.

3.2. ZQGCD improves IDD and hyperalgesia in rats

Compared with the model group, the PWT threshold of rats in ZQGCD high-dose groups was significantly increased on the 25th day ($P < 0.001$), and the PWL threshold of rats in ZQGCD low, medium, and high-dose groups was significantly increased ($P < 0.01$, $P < 0.01$, $P < 0.0001$). The results indicated that ZQGCD could improve hyperalgesia in IDD model rats (Fig. 2A and B).

The expression of the inflammatory neuropeptide substance P protein in intervertebral disc tissues of rats in the model group was significantly increased ($P < 0.0001$). However, in the ZQGCD medium and high dose groups, a significant decrease in the expression of substance P was observed when compared with the model group ($P < 0.0001$, $P < 0.0001$). These findings suggest that ZQGCD effectively inhibits the expression of inflammatory neuropeptides in the degenerated intervertebral disc of IDD rats (Fig. 2C and Fig. S1).

In the sham group, the NP exhibited fullness, with a clear boundary to the AF, presenting a structurally complete and orderly AF. Conversely, in the model group, the NP of rats displayed evident wrinkling, the structure was disordered, and the AF was locally torn

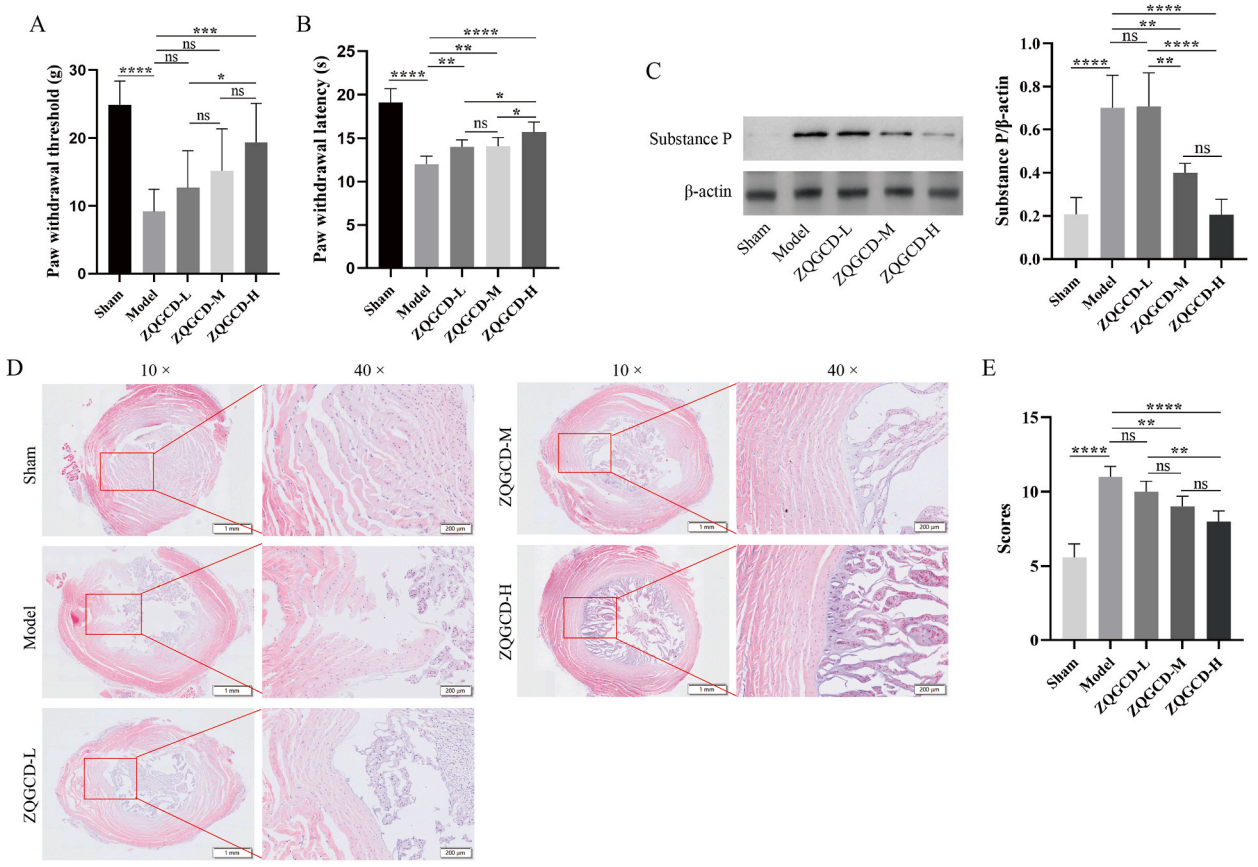

Fig. 2. The impact of ZQGCD on IDD rats. (A) Paw withdrawal threshold in rats. (B) Paw withdrawal latency in rats. (C) Relative expression level of substance P protein in intervertebral disc tissue of rats. The unedited images are referenced in Fig. S1 (D) Representative HE-stained intervertebral disc sections (magnification: 10 × or 40 ×). (E) Intervertebral disc histopathologic score. *: $P < 0.05$, **: $P < 0.01$, ***: $P < 0.001$, ****: $P < 0.0001$, ns: $P > 0.05$.

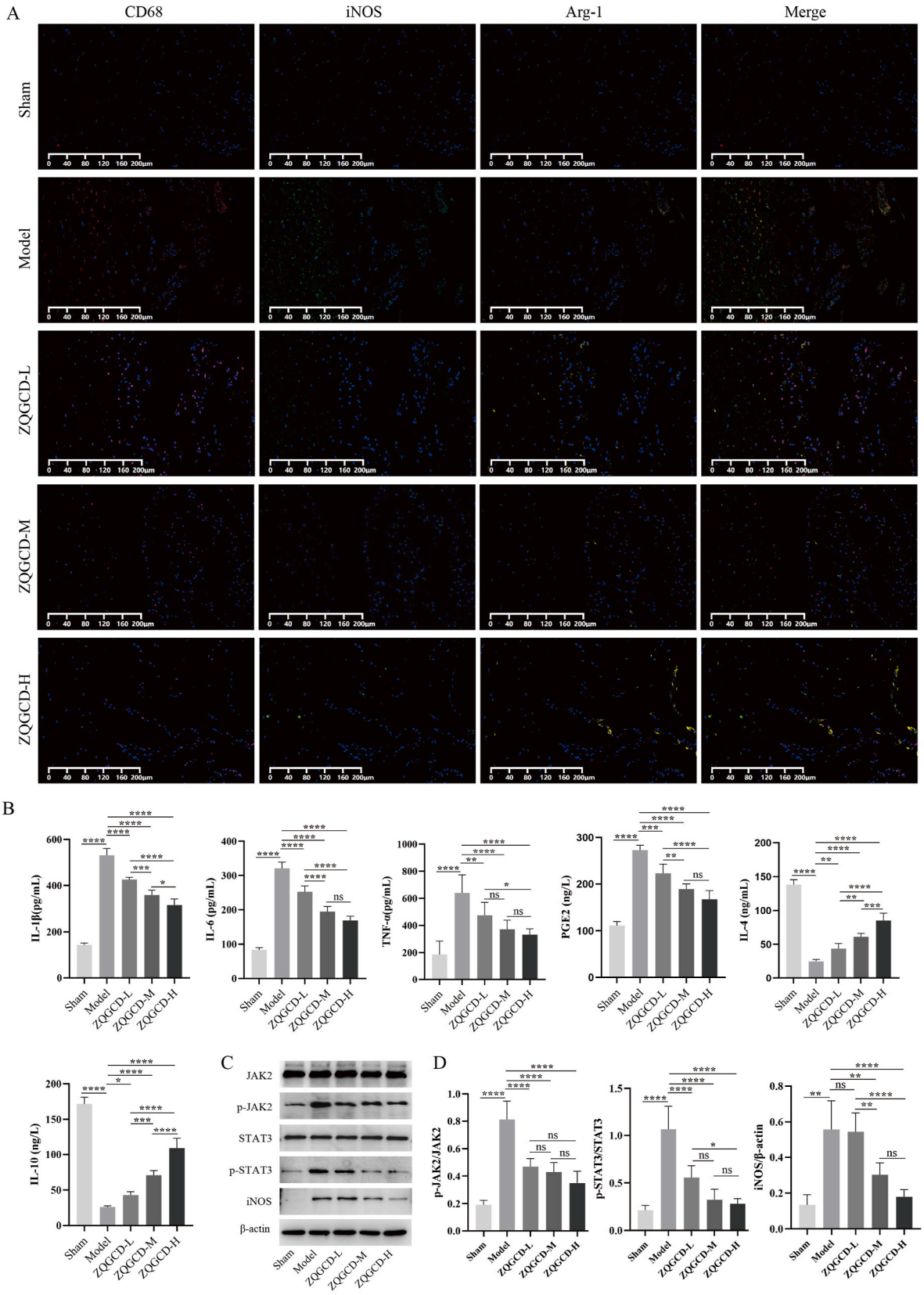

(caption on next page)

Fig. 3. Effect of ZQGCD on the polarization direction of macrophages and JAK2/STAT3 pathway in intervertebral disc of IDD rats. (A) Multiple immunofluorescence staining of intervertebral discs. (B) Comparison of the expression levels of serum IL-1β, IL-6, TNF-α, PEG2, IL-4, and IL-10. (C, D) The relative expression levels of *p*-JAK2/JAK2, p-STAT3/STAT3, iNOS/β-actin in the interdisc tissues of rats in each group. The unedited images are referenced in Fig. S2. *: $P < 0.05$, **: $P < 0.01$, ***: $P < 0.001$, ****: $P < 0.0001$, ns: $P>0.05$.

and disordered. In the ZQGCD low and medium dose groups, more than half of the NP of rats collapsed, the structure was disordered, and a nake-like fibrous ring appeared. Notably, the ZQGCD high-dose group exhibited partial NP wrinkling, with a clear boundary to the AF, maintaining an intact AF structure and a normal arrangement. Comparisons with the sham operation group revealed a significantly higher histopathologic score of model rats ($P < 0.0001$). Conversely, when compared with the model group, the histopathologic scores of intervertebral disc tissue in ZQGCD medium and high dose groups were significantly decreased ($P < 0.01$, $P < 0.0001$) (Fig. 2D and E).

3.3. Effect of ZQGCD on macrophage polarization and JAK2/STAT3 pathway in intervertebral disc of IDD rats

CD68 serves as a macrophage marker, iNOS as an M1 macrophage marker, and Arg-1 as an M2 macrophage marker. Double positivity for CD68 and iNOS indicated M1 polarization, while CD68 and Arg-1 double indicated M2 polarization. In the model group, there was a significant influx of macrophage into the intervertebral disc of rats predominantly M1 type. Serum levels of pro-inflammatory factors IL-1β, IL-6, TNF-α, and angiogenic factor PEG2 were significantly elevated, whereas anti-inflammatory factors IL-4 and IL-10 were significantly decreased. Compared to the model group, ZQGCD treatment reduced macrophage infiltration in the intervertebral significantly decreasing M1 macrophages while increasing M2 macrophages. Serum levels of IL-1β, IL-6, TNF-α, and PEG2 decreased ($P < 0.05$), while IL-4 and IL-10 levels increased ($P < 0.05$) (Fig. 3A and B).

Compared with the sham group, protein expressions of *p*-JAK2, p-STAT3, and iNOS in the intervertebral disc tissues of the model group were significantly elevated ($P < 0.01$). Conversely, compared with the model group, ZQGCD treatment led to decreased protein expressions of *p*-JAK2, p-STAT3, and iNOS in the intervertebral disc tissue of rats ($P < 0.05$). These findings indicate that ZQGCD can inhibit the expression of the JAK2/STAT3/M1 polarization pathway in the degenerated intervertebral disc of IDD rats (Fig. 3C, D, and Fig. S2).

3.4. Effects of ZQGCD on macrophage proliferation and migration in vitro

When macrophages were cultured with different concentrations of blank serum and ZQGCD-containing serum for 24 h, there was no significant difference in cell activity between equivalent concentrations of both the blank serum and ZQGCD-containing serum groups ($P>0.05$). This suggested that ZQGCD-containing serum did not exert a promoting effect on macrophage proliferation (Fig. 4A). The effect of ZQGCD-containing serum on macrophage migration was determined using a scratch test. After culturing macrophages

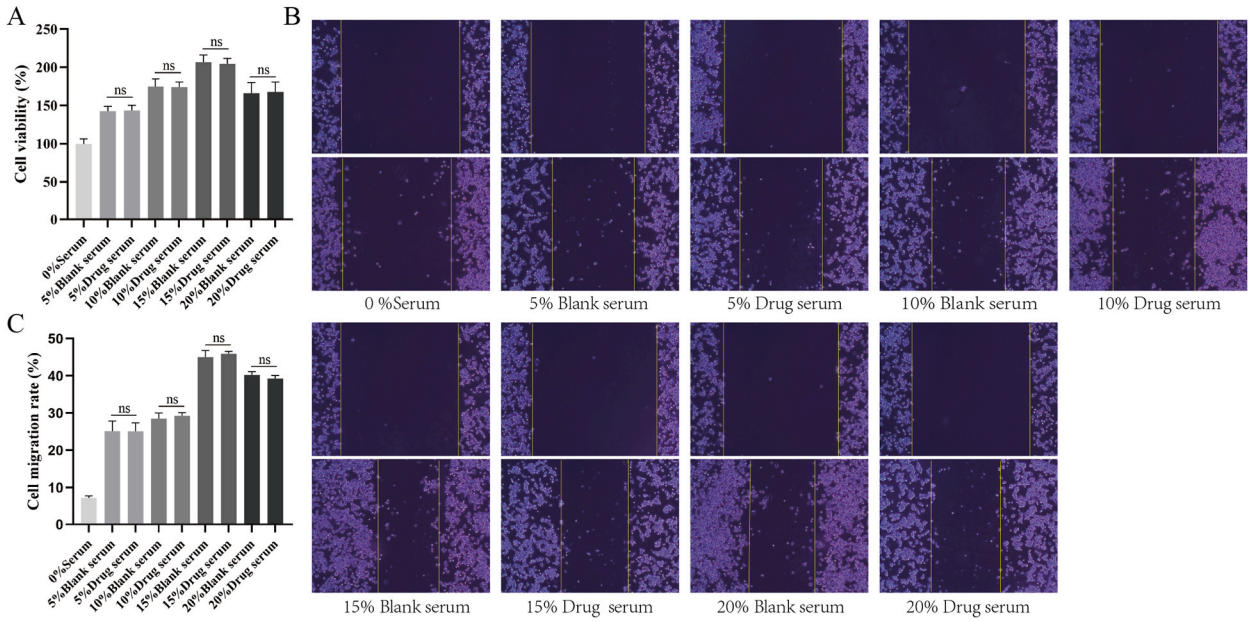

Fig. 4. The effect of ZQGCD on the proliferation and migration of macrophages in vitro. (A) Comparison of the macrophage activity between different concentrations of blank serum and ZQGCD serum cultured for 24 h. (B) Macrophage migration was examined under light microscope after exposure to different concentrations of blank serum and ZQGCD serum for 24 h. (C) Comparison of macrophage mobility. ns: $P>0.05$.

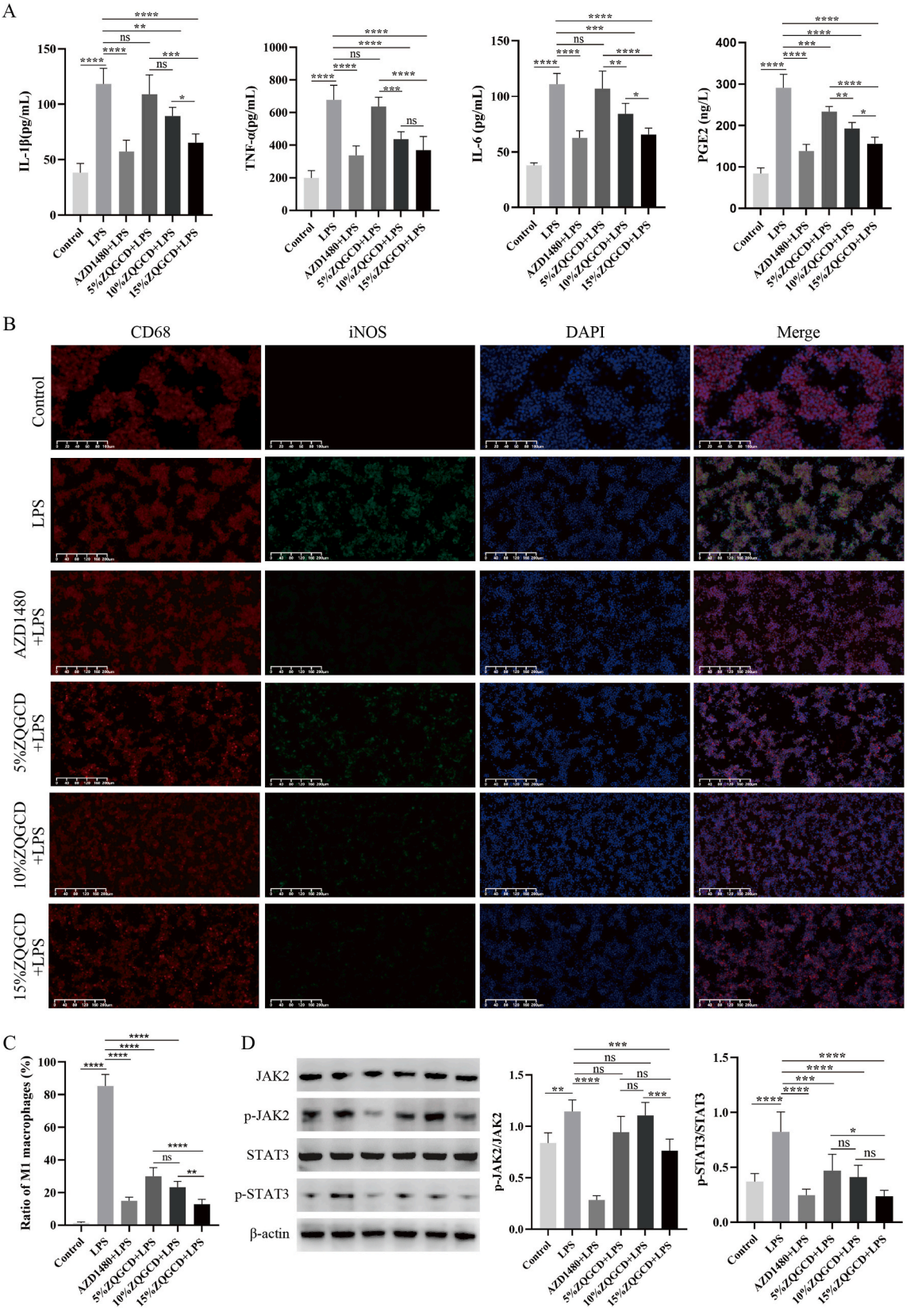

(caption on next page)

Fig. 5. ZQGCD-containing serum inhibits LPS-induced M1 polarization of macrophages by regulating the JAK2/STAT3 pathway. (A) Expression levels of IL-1β, IL-6, TNF-α and PEG2 in macrophage supernatant. (B) M1 polarization of macrophages examined by multiple immunofluorescence. (C) The proportion of M1 macrophages. (D) Relative expression of *p*-JAK2/JAK2, p-STAT3/STAT3 in macrophages. The unedited images are referenced in Fig. S3. *: $P < 0.05$, **: $P < 0.01$, ***: $P < 0.001$, ****: $P < 0.0001$, ns: $P>0.05$.

with different concentrations of blank serum and ZQGCD-containing serum for 24 h, there was no significant difference in cell mobility between the same concentrations of the blank serum and ZQGCD-containing serum groups ($P>0.05$). The results indicate that ZQGCD did not induce macrophage migration (Fig. 4B and C).

3.5. *ZQGCD-containing serum modulates the JAK2/STAT3 pathway to inhibit LPS-induced M1 macrophage polarization*

Compared to the control group, the levels of IL-1β, IL-6, TNF-α, and PEG2 in the LPS group were significantly increased ($P < 0.0001$). Conversely, in the JAK2 inhibitor (AZD1480+LPS) group and ZQGCD-containing serum groups (10 % ZQGCD + LPS and 15 % ZQGCD + LPS), the levels of IL-1β, IL-6, TNF-α, and PEG2 were significantly reduced ($P < 0.01$) (Fig. 5A). Immunofluorescence demonstrated that LPS induced M1 polarization in undifferentiated macrophages. Notably, both the AZD1480+LPS group and the 10 % ZQGCD + LPS group, as well as the 15 % ZQGCD + LPS group, effectively inhibited M1 polarization of macrophages (Fig. 5B and C). Compared with the control group, the protein expressions of *p*-JAK2 and p-STAT3 in macrophages significantly increased after LPS induction ($P < 0.001$). However, the expression of *p*-JAK2 and p-STAT3 proteins in macrophages of the AZD1480+LPS and ZQGCD + LPS groups was decreased ($P < 0.05$) (Fig. 5D, and Fig. S3). These results indicate that both JAK2 inhibitors and ZQGCD can inhibit the

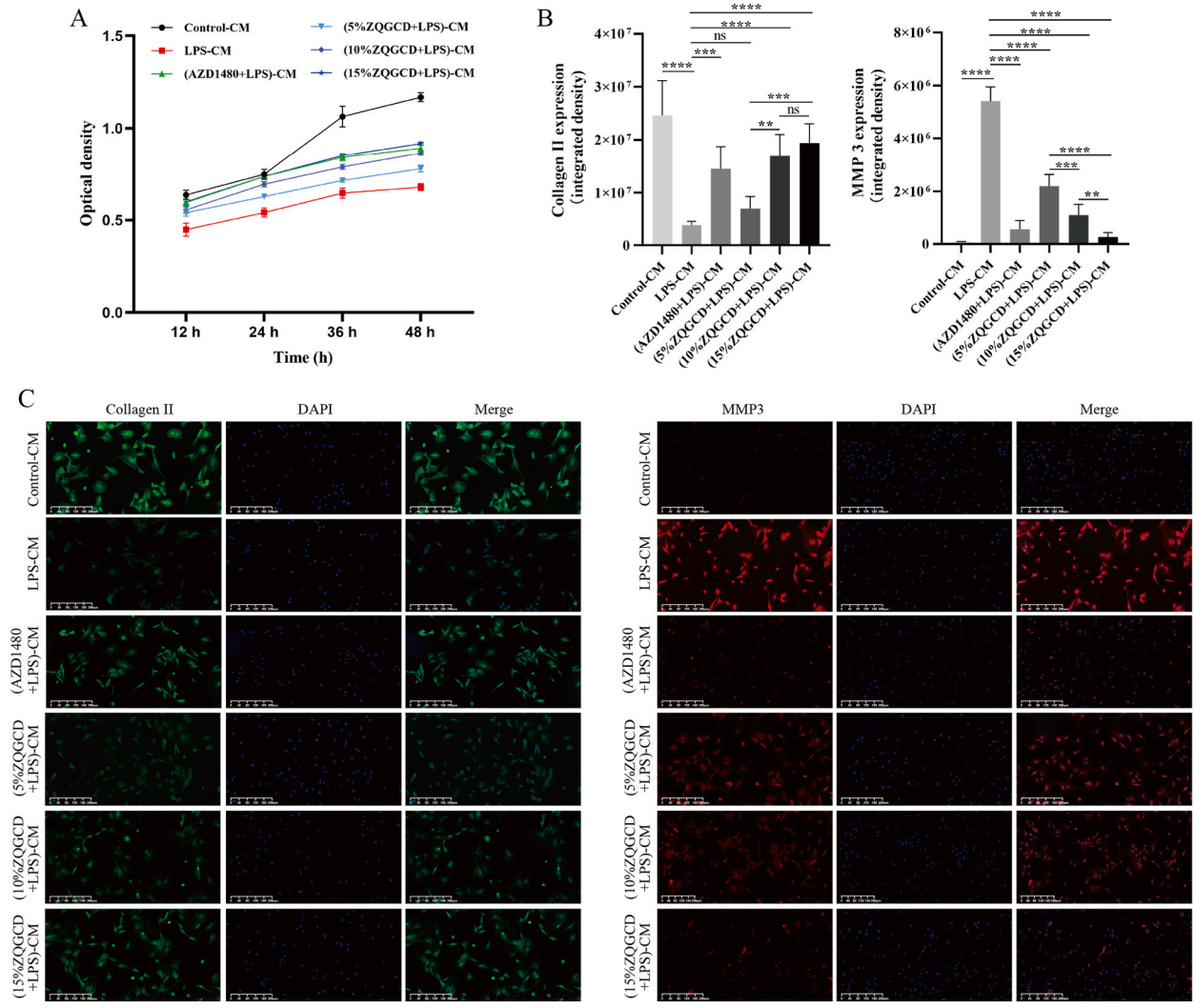

Fig. 6. Effect of macrophage conditioned medium on NPCs. (A) A line chart of NPCs activity. (B, C) Relative expression of collagen II and MMP3 in NPCs was detected by immunofluorescence. *: $P < 0.05$, **: $P < 0.01$, ***: $P < 0.001$, ****: $P < 0.0001$, ns: $P>0.05$.

JAK2/STAT3 pathway, thereby inhibiting the M1 macrophage polarization.

3.6. Effect of macrophage-conditioned medium on NPCs

When cultured with LPS macrophage supernatant as a conditioned medium, the growth of NPCs was significantly inhibited, and the expression of the extracellular matrix synthesizing gene collagen II was significantly decreased ($P < 0.0001$). Simultaneously, the expression of the extracellular matrix-degrading gene MMP3 showed a significant increase ($P < 0.0001$). Compared to the LPS group, 48 h after culturing with macrophage supernatant from the AZD1480 group and ZQGCD-containing serum groups, the activity of NPCs and the expression of collagen II were higher, while the expression level of MMP3 was lower. ($P < 0.01$) (Fig. 6A, B, and C).

4. Discussion

When intervertebral disc degeneration, AF rupture, or NP herniation takes place, it leads to the breakdown of the physical barrier separating the intervertebral disc from the immune system. As a result, the immune system becomes exposed to the NP [25]. Afterwards, the immune system identifies the NP as an "alien antigen" with "immune privilege", triggering an initial immune reaction. After the damaged NP and AF are repaired, granulation tissue forms, followed by blood vessel growth, further exposing the NP tissue to immune cells [26]. In this scenario, certain portions of the NP matrix are identified as autoantigens, leading to the activation of a secondary immune response facilitated by immune cells [5]. The level of tissue inflammation is mainly influenced by the condition of macrophages, specifically the equilibrium between the transformation of macrophages into pro-inflammatory M1 macrophages and anti-inflammatory M2 macrophages, as a result of the inherent immune response [27]. IDD can be delayed by inhibiting the polarization of macrophage M1 due to their high plasticity, which allows them to adapt to environmental stimuli and alter their phenotype [28]. In the degenerated intervertebral disc tissue of model rats, the study uncovered infiltration of M1 macrophages. There was an increase in the production of proinflammatory and pain-causing substances, a decrease in the production of anti-inflammatory substances, an increase in the production of substance P (an inflammatory neuropeptide) in the tissue of intervertebral discs, and as a result, the rats showed hyperalgesia.

ZQGCD, included in China's National Famous Medical Secret Prescription, is primarily used for the treatment of spinal diseases with proven clinical efficacy. In this study, LC-MS/MS technology identified 81 active components of ZQGCD, providing a preliminary understanding of its material basis. Among them, Narirutin, Ferulic Acid, Tanshinone IIA, Germacrone, Kanokoside, and Caffeate are the quality control index components of Aurantii fructus, Angelicae sinensis radix, Radix salviae miltiorrhizae, Curcumae rhizome, Glycyrrhizae radix et rhizoma, Pharbitidis, and Pharbitis purpurea, respectively, as specified of the Chinese Pharmacopoeia. These components can serve as candidate indicators for quality control of ZQGCD in the future. Narirutin is a dihydroflavonoid compound, which is widely distributed in Aurantii fructus, Citrus aurantium L. and Exocarpium citrl Grandis. Modern pharmacological studies have revealed that Narirutin has multiple effects such as anti-oxidation, anti-inflammation, anti-osteoporosis and regulation of blood lipids [29]. Narirutin exerts its anti-inflammatory activity by suppressing NLRP3 inflammasome activation via inhibition of the NLRP3 inflammasome priming processes and NLRP3-ASC interaction in macrophages [30]. Ferulic acid is a phenolic substance found in many Chinese medicines. Its chemical name is (E)-3-(4-hydroxy-3-methoxyphenyl)prop-2-enoic acid. Ferulic acid has been proved to have anti-oxidative stress, anti-inflammation, anti-apoptosis, anti-platelet aggregation and other biological activities [31]. Studies have shown that platelet-rich plasma and ferulic acid hydrogel compound have a positive effect on promoting extracellular matrix synthesis and repairing IDD in rats [32]. Salvia miltiorrhiza is a traditional Chinese medicine for promoting blood circulation and removing blood stasis. Tanshinone IIA is a fat-soluble component of Radix salviae miltiorrhizae. It has anti-inflammatory, antioxidant, anti-platelet aggregation, anti-tumor and other pharmacological effects [33]. By inhibiting p38 MAPK signaling pathway, sodium tanshinone IIA sulfonate IDD model rats and showed anti-inflammatory and anti-oxidant properties [34]. Gemalone is a natural sesquiterpenoid compound mainly derived from Curcumae rhizome. Modern studies have confirmed that Gemalone has a significant anti-tumor effect, can be used in the treatment of liver cancer, stomach cancer, breast cancer and other malignant tumors, but also has a wide range of antioxidant, anti-inflammatory, antiviral effects [35]. Studies have shown that Germarone alleviates collagen-induced arthritis by regulating the NF-κB signaling pathway and T helper cell type (Th) 1/Th2 balance [36]. The mechanism by which ZQGCD exerts its therapeutic effect is likely related to the synergistic effect of these compounds.

Following ZQGCD treatment, infiltrating macrophages in intervertebral disc tissues of model rats decreased, the content of M1 macrophages decreased, while the content of M2 macrophages increased, the expression of proinflammatory factors and pain-inducing factors in serum decreased, and the expression of substance P in intervertebral disc tissue decreased. Consequently, the intervertebral disc degeneration and hyperalgesia of rats were improved. The degree of these changes was found to be dosage-dependent for ZQGCD. These results suggest that the mechanism of ZQGCD in treating IDD may be related to the regulation of macrophage polarization.

The JANUS kinase/signal transduction and transcriptional activator (JAK/STAT) signal is the primary signal transduction pathway for cytokines, playing a pivotal role in initiating innate immunity and coordinating adaptive immune responses [37]. This pathway is an important regulator of macrophage polarization, where the activation of JAK1/2 and STAT1/3 mediates M1 polarization, while the activation of JAK1/3 and STAT6 mediates M2 polarization [38]. In vivo studies demonstrated increased expression of the JAK2/STAT3 signaling pathway in the degraded disc tissues of model rats, suggesting the involvement of JAK/STAT-mediated macrophage polarization in the disc degeneration process. In vitro studies revealed that LPS induced M1 macrophage polarization. Both JAK2 inhibitors and ZQGCD inhibited M1 polarization by inhibiting the JAK2/STAT3 pathway. Polarized macrophages, as a result, released a significant amount of inflammatory factors, including IL-1β, IL-6, and TNF-α, which inhibited the proliferation and collagen II secretion of NPCs and promoted the secretion of MMP3, consequently contributing to NPCs degeneration. Both JAK2 inhibitors and

ZQGCD demonstrated the ability to inhibit M1 polarization, thereby reducing the levels of IL-1β, IL-6, TNF-α, and other inflammatory factors. Consequently, this inhibition led to a delay in the degeneration of NPCs.

5. Conclusion

This study revealed the presence of macrophage infiltration in the intervertebral disc tissue of IDD rats. Moreover, the JAK2/STAT3 pathway is activated, and the macrophages are polarized towards the M1 phenotype. This phenotypic shift contributes to the establishment of an inflammatory microenvironment, ultimately contributing to intervertebral disc degeneration and the onset of hyperalgesia. ZQGCD exerts a mitigating effect on IDD and improves hyperalgesia in model rats by inhibiting the JAK2/STAT3/macrophage M1 polarization pathway. (Fig. 7).

Funding

This work was supported by the National Natural Science Foundation of China (82174399), the Natural Science Foundation of Jiangsu province (BK20220260, BK20211084), TCM Science and Technology Development Program of Jiangsu Province (QN202007, QN202222), Suzhou science and technology development plan project (SKYD2023150), Construction project of Key Laboratory of Bone Injury Science of Traditional Chinese Medicine (JSDW202253, SZS2022019), Jiangsu Provincial Medical Key Discipline(Laboratory) Cultivation Unit (Suzhou Health Science and Education [2022] No. 17), and the seventh batch of national traditional Chinese medicine experts academic experience inheritance work project (Chinese Medicine Education Letter [2022] No. 76).

Data availability statement

The original contributions presented in the study are included in the article and supplement files, further inquiries can be directed to the corresponding authors.

Ethics approval and consent to participate

The Medical Ethics Committee of Suzhou TCM Hospital approved all experimental procedures (2020-060).

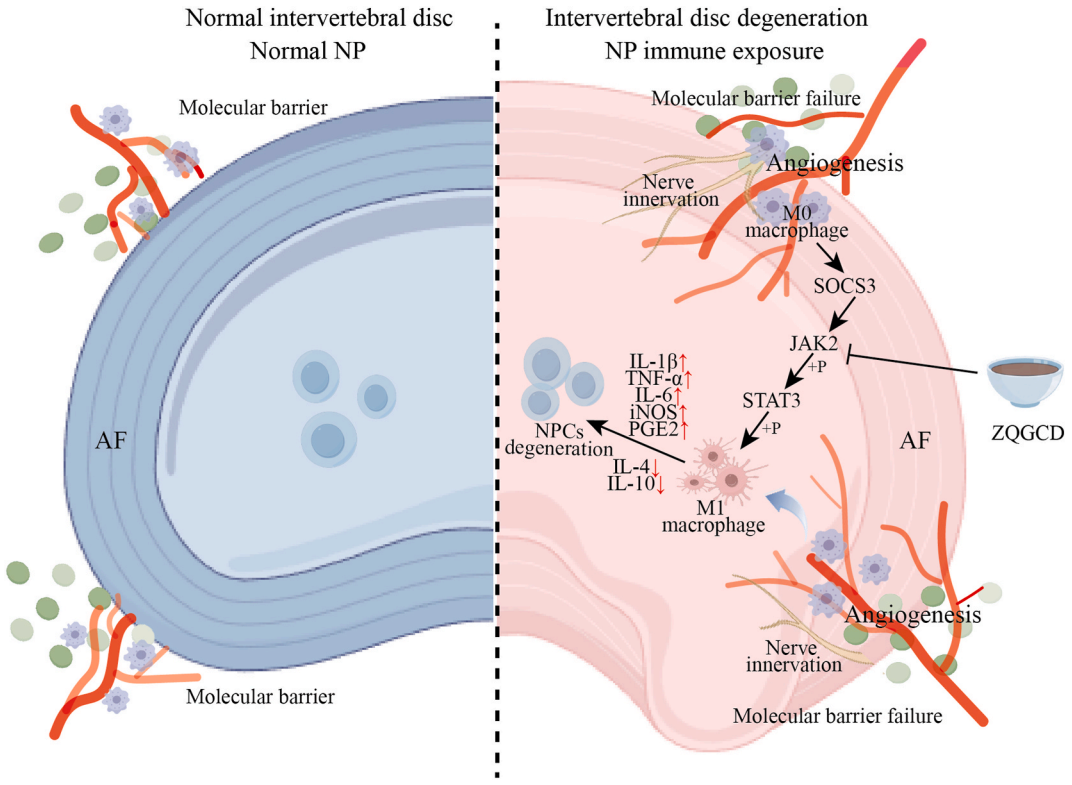

Fig. 7. Schematic summary illustration. AF: annulus fibrosus, NP: nucleus pulposus, NPCs: nucleus pulposus cells, ZQGCD: Zhiqiao Gancao decoction.

Consent for publication

Not applicable.

CRediT authorship contribution statement

Zeling Huang: Writing – original draft, Formal analysis, Data curation, Conceptualization. **Xiaofeng Shen:** Writing – original draft, Data curation, Conceptualization. **Hua Chen:** Methodology, Investigation, Formal analysis, Data curation. **Zaishi Zhu:** Software, Methodology, Investigation. **Binjie Lu:** Methodology, Investigation. **Long Zhang:** Supervision, Software. **Yujiang Liu:** Validation, Supervision. **Yuwei Li:** Writing – review & editing, Visualization, Supervision, Funding acquisition. **Bo Xu:** Writing – review & editing, Project administration, Funding acquisition, Conceptualization.

Declaration of competing interest

The authors declare that they have no conflicts of interest to disclose.

Acknowledgments

We thank for the help provided by the Key Laboratory for Metabolic Diseases in Chinese Medicine, First College of Clinical Medicine, Nanjing University of Chinese Medicine, and the language editing service for Home for Researchers editorial team (www.home-for-researchers.com).

List of abbreviations

AF	Annulus fibrosus
CM	Conditioned medium
IL	Interleukin
IDD	Intervertebral disc degeneration
LBP	Low back pain
LC-MS/MS	Liquid chromatography-tandem mass spectrometry
LPS	Lipopolysaccharides
ZQGCD	Zhiqiao Gancao decoction
MMP3	Matrix metalloproteinase-3
NEG	Negative ion mode
NP	Nucleus pulposus
NPCs	Nucleus pulposus cells
PWL	Paw retraction latency
PWT	Paw withdrawal threshold
POS	Positive ion mode
TNF-α	Tumor necrosis factor-α

Appendix A. Supplementary data

Supplementary data to this article can be found online at https://doi.org/10.1016/j.heliyon.2024.e34715.

References

[1] N.N. Knezevic, K.D. Candido, J.W.S. Vlaeyen, Z.J. Van, S.P. Cohen, Low back pain, Lancet. 398 (10294) (2021) 78–92.
[2] M.J. DePalma, J.M. Ketchum, T. Saullo, What is the source of chronic low back pain and does age play a role? Pain Med. 12 (2) (2011) 224–233.
[3] N. Bogduk, C. Aprill, R. Derby, Lumbar discogenic pain: state-of-the-art review, Pain Med. 14 (2013) 813–836.
[4] T. Takada, K. Nishida, M. Doita, M. Kurosaka, Fas ligand exists on intervertebral disc cells: a potential molecular mechanism for immune privilege of the disc, Spine 27 (2002) 1526–1530.
[5] S. Kaneyama, K. Nishida, T. Takada, T. Suzuki, T. Shimomura, K. Maeno, et al., Fas ligand expression on human nucleus pulposus cells decreases with disc degeneration processes, J. Orthop. Sci. 13 (2) (2008) 130–135.
[6] S. Kobayashi, A. Meir, Y. Kokubo, K. Uchida, K. Takeno, T. Miyazaki, et al., Ultrastructural analysis on lumbar disc herniation using surgical specimens: role of neovascularization and macrophages in hernias, Spine 34 (7) (2009) 655–662.
[7] A. Shapouri-Moghaddam, S. Mohammadian, H. Vazini, M. Taghadosi, S.A. Esmaeili, F. Mardani, et al., Macrophage plasticity, polarization, and function in health and disease, J. Cell. Physiol. 233 (9) (2018) 6425–6440.
[8] S. Lee, M. Millecamps, D.Z. Foster, L.S. Stone, Long-term histological analysis of innervation and macrophage infiltration in a mouse model of intervertebral disc injury-induced low back pain, J. Orthop. Res. 38 (6) (2020) 1238–1247.
[9] J. Virri, M. Grönblad, S. Seitsalo, A. Habtemariam, E. Kääpä, E. Karaharju, Comparison of the prevalence of inflammatory cells in subtypes of disc herniations and associations with straight leg raising, Spine 26 (21) (2001) 2311–2315.

[10] S. Kadomoto, K. Izumi, A. Mizokami, Macrophage polarity and disease control, Int. J. Mol. Sci. 23 (1) (2021) 144.
[11] J. Koroth, E.O. Buko, R. Abbott, C.P. Johnson, B.M. Ogle, L.S. Stone, et al., Macrophages and intervertebral disc degeneration, Int. J. Mol. Sci. 24 (2) (2023) 1367.
[12] T. Takada, K. Nishida, K. Maeno, K. Kakutani, T. Yurube, M. Doita, et al., Intervertebral disc and macrophage interaction induces mechanical hyperalgesia and cytokine production in a herniated disc model in rats, Arthritis Rheum. 64 (8) (2012) 2601–2610.
[13] X.C. Li, S.J. Luo, W. Fan, T.L. Zhou, D.Q. Tan, R.X. Tan, et al., Macrophage polarization regulates intervertebral disc degeneration by modulating cell proliferation, inflammation mediator secretion, and extracellular matrix metabolism, Front. Immunol. 13 (2022) 922173.
[14] D.J. Gorth, I.M. Shapiro, M.V. Risbud, Transgenic mice overexpressing human TNF-alpha experience early onset spontaneous intervertebral disc herniation in the absence of overt degeneration, Cell Death Dis. 10 (1) (2018) 7.
[15] C. Chen, Y.W. Li, H. Chen, Clinical study on Zhiqiao Gancao decoction for treatment of lumbar disc herniation, Chinese Journal of Traditional Chinese Medicine 29 (5) (2014) 752–753.
[16] X.C. Tang, Z.F. Gong, Y.W. Li, Clinical observation of Zhiqiao Gancao decoction treating 26 cases of lumbar and leg pain in young and middle-aged patients, Clinical Journal of Chinese Medicine 8 (31) (2016) 59–60+62.
[17] X.F. Shen, L. Li, Q.H. Ma, Pharmacokinetic study of eight bioactive components following oral administration of Zhiqiao Gancao decoction and observation of its clinical efficacy, Biomed. Chromatogr. 34 (2) (2020) e4706.
[18] Y.J. Liu, S.L. Wang, X.F. Cai, X. Bo, J. Lin, Y.W. Li, To observe the clinical effect of Zhiqiao Gancao decoction on lumbar disc herniation based on Pfirrmann grading, Journal of Zhejiang Chinese Medical University 47 (6) (2023) 651–658.
[19] T.S. Cang, Y. Chen, Y.W. Li, Zhiqiao Gancao Decoction combined with lumbar traction for the improvement of lumbar disc herniation, World of Traditional Chinese Medicine 15 (13) (2020) 1981–1984.
[20] J.T. Sun, Y.W. Li, X.F. Shen, H. Chen, Effects of Zhiqiao Gancao Decoction on inflammation and degeneration of lumbar disc herniation model rats, Chinese Journal of Emergency of Traditional Chinese Medicine 25 (8) (2016) 1488–1492.
[21] X.F. Shen, Z.F. Gong, G.Q. Liang, Effects of Zhiqiao Gancao Decoction on acid-sensitive ion channels and related factors in rats with lumbar disc Herniation, Journal of Liaoning University of Traditional Chinese Medicine 22 (1) (2020) 36–39.
[22] Z.L. Huang, B.J. Lu, X.D. Zhang, J.P. Wang, X.F. Cai, Y.J. Liu, et al., Zhiqiao Gancao decoction ameliorates hyperalgesia in lumbar disc herniation via the CCL2/CCR2 signaling pathway, Drug Des. Dev. Ther. 17 (2023) 2239–2257.
[23] F. Chen, S. Lu, N. Li, Advances in the development of intervertebral disc degeneration models, Orthop. J. China, 30 (9) (2022) 821–825.
[24] K. Masuda, Y. Aota, C. Muehleman, Y. Imai, M. Okuma, E.J. Thonar, et al., A novel rabbit model of mild, reproducible disc degeneration by an anulus needle puncture: correlation between the degree of disc injury and radiological and histological appearances of disc degeneration, Spine 30 (1) (2005) 5–14.
[25] M. Stefanakis, M. Al-Abbasi, I. Harding, Annulus fissures are mechanically and chemically conducive to the ingrowth of nerves and blood vessels, Spine 37 (2012) 1883–1891.
[26] F. Ye, F.J. Lyu, H. Wang, Z.M. Zheng, The involvement of immune system in intervertebral disc herniation and degeneration, JOR Spine 5 (1) (2022) e1196.
[27] Z. Sun, B. Liu, Z.J. Luo, The immune privilege of the intervertebral disc: implications for intervertebral disc degeneration treatment, Int. J. Med. Sci. 17 (5) (2020) 685–692.
[28] C. Song, W.Y. Cai, F. Liu, K. Cheng, D. Guo, Z.C. Liu, An in-depth analysis of the immunomodulatory mechanisms of intervertebral disc degeneration, JOR Spine 5 (4) (2022) e1233.
[29] S. Mitra, M.S. Lami, T.M. Uddin, R. Das, F. Islam, J. Anjum, et al., Prospective multifunctional roles and pharmacological potential of dietary flavonoid narirutin, Biomed. Pharmacother. 150 (2022) 112932.
[30] M.H. Ri, M.Y. Li, Y. Xing, H.X. Zuo, G. Li, C. Li, J. Ma, et al., Narirutin exerts anti-inflammatory activity by inhibiting NLRP3 inflammasome activation in macrophages, Phytother Res. 37 (4) (2023) 1293–1308.
[31] D. Li, Y.X. Rui, S.D. Guo, F. Luan, R. Liu, N. Zeng, Ferulic acid: a review of its pharmacology, pharmacokinetics and derivatives, Life Sci. 284 (2021) 119921.
[32] Q. Chai, B.N. Zhang, Y.F. Da, W.W. Wang, Y.D. Gao, M.Y. Yao, et al., Enhancement and repair of degenerative intervertebral disc in rats using platelet-rich plasma/ferulic acid hydrogel, Cartilage 14 (4) (2023) 506–515.
[33] R. Guo, L. Li, J. Su, S. Li, S.E. Duncan, Z.H. Liu, et al., Pharmacological activity and mechanism of tanshinone IIA in related diseases, Drug Des. Dev. Ther. 14 (2020) 4735–4748.
[34] S.Q. Dai, X. Shi, R.Q. Qin, X. Zhang, F. Xu, H.L. Yang, Sodium tanshinone IIA sulfonate ameliorates injury-induced oxidative stress and intervertebral disc degeneration in rats by inhibiting p38 MAPK signaling pathway, Oxid. Med. Cell. Longev. 2021 (2021) 5556122.
[35] G.H. Lou, Y. Huang, Y. Wang, S.Y. Chen, C. Liu, Y. Li, et al., Germacrone, A novel and safe anticancer agent from genus curcuma: a review of its mechanism, Anti Cancer Agents Med. Chem. 23 (13) (2023) 1490–1498.
[36] Z.R. Wang, F. Zhuo, P.G. Chu, X.L. Yang, G. Zhao, Germacrone alleviates collagen-induced arthritis via regulating Th1/Th2 balance and NF-κB activation, Biochem. Biophys. Res. Commun. 18 (3) (2019) 560–564.
[37] X.Y. Hu, J. Li, M.R. Fu, X. Zhao, W. Wang, The JAK/STAT signaling pathway: from bench to clinic, Signal Transduct Target Ther 6 (1) (2021) 402.
[38] Z. Yan, S.A. Gibson, J.A. Buckley, H. Qin, E.N. Benveniste, Role of the JAK/STAT signaling pathway in regulation of innate immunity in neuroinflammatory diseases, Clin Immunol 189 (2018) 4–13.